DOI: https://doi.org/10.4038/engineer.v58i2.7692
ENGINEER - Vol. LVIII, No. 02, pp. [35-48], 2025

Numerical Evaluation of the Static Performance of Solid Resilient Tires by Varying Key Parameters

B.Y. Wickramasuriya and J.A.S.C. Jayasinghe

Abstract: Solid tires are a significant engineering innovation used in a variety of applications. In industrial settings, they are found on large tractors, trucks, heavy loading equipment, and smaller machinery like forklifts, bike tires, lawnmowers, and casters. Numerous studies have simulated the behaviour of solid tires under both static and dynamic conditions. The goal of this study is to develop a numerical approach to understand how changes in layer thickness and bead wire percentage affect the static performance of solid tires. In this study, rubber components were modelled using a hyper-elastic material model. The most suitable hyper-elastic model was identified in *ABAQUS* by utilizing experimental data and a curve-fitting approach. The Yeoh hyper-elastic material model exhibited the lowest statistical errors, as measured by the Mean Absolute Percentage Error (MAPE), Mean Signed Difference (MSD), and Mean Absolute Deviation (MAD). The static numerical model, developed using the best-fitting hyper-elastic material model, was validated against the experimental data obtained. Next, a parametric study was conducted with two case studies: altering the material properties of different layers and varying the percentage of bead wires. In the first parametric study, which involved altering the material properties of the layers, the model with base layer and tread layer as cushion material properties (CCC) significantly increases displacements, achieving a 66 % increment in vertical displacement and a 73 % increment in horizontal displacement. Additionally, the model with cushion layer with base material (BBT) model demonstrates a 13 % decrease in contact area relative to the original model. In the second parametric study focused on changing the percentage of bead wires, minimal variation was observed in the static performance outcomes. Therefore, it is recommended to conduct a dynamic analysis to further investigate the impact of reinforcement variation. These results provide a more detailed understanding of the static performance of solid resilient tires in relation to key tire parameters that benefit the solid tire industry.

Keywords: Bead wire, Hyper-elastic material model, Nonlinear finite element simulation, Solid resilient tire, Static performance

1. Introduction

A solid tire, also known as an airless tire, is a type of tire that is not supported by air pressure. Unlike pneumatic tires as shown in Figure 1 (a), solid tires are made entirely of solid rubber or a similar resilient material. The significance of solid tires lies in their durability and resistance to punctures, making them ideal for harsh working environments. Solid tires are widely used in industrial applications, particularly in forklifts, heavy-duty construction equipment, and military vehicles, where reliability and longevity are paramount.

In Sri Lanka, the solid tire industry plays a crucial role in the economy. The country is one of the leading exporters of solid tires, leveraging its abundant natural rubber resources. The industry has grown significantly over the past few decades, driven by advancements in manufacturing technologies and increasing global demand for robust and reliable tire solutions. The presence of well-established rubber plantations and skilled labour has positioned Sri Lanka as a key player in the global solid tire market.

Solid tires are composed of multiple layers as shown in Figure 1 (b), each serving a specific function to enhance the tire's performance and durability. The primary layers included in solid tire are the tread, base, cushion, and bead wires. The tread layer is the outermost layer, designed to provide traction and resist wear. It is typically made of a tough rubber compound that can withstand abrasive surfaces and harsh conditions. The base layer, located beneath the cushion layer, offers additional strength and stability, helping to distribute loads evenly across the tire and reducing stress to extend the

***Eng. B.Y.Wickramasuriya**, AMIE(SL), B.Sc. Eng. (Hons) (Peradeniya), Department of Civil Engineering, Faculty of Engineering, University of Peradeniya.*
Email:yasaswickramasuriya97@gmail.com
ORCID ID:https://orcid.org/0009-0003-0358-1023
***Eng. (Dr.)J.A.S.C. Jayasinghe**, AMIE(SL), B.Sc. Eng. (Hons) (Peradeniya), M.Eng. (AIT), PhD. (Tokyo), Senior Lecturer in Department of Civil Engineering, University of Peradeniya, Sri Lanka.*
Email:supunj@pdn.ac.lk
ORCID ID:http://orcid.org/0000-0003-1054-9358

tire's lifespan. The cushion layer, positioned between the base and the bead wires, provides shock absorption and improves ride comfort by dampening vibrations and impacts. The bead wires, the innermost components, secure the tire to the wheel rim, ensuring a tight fit and preventing slippage.

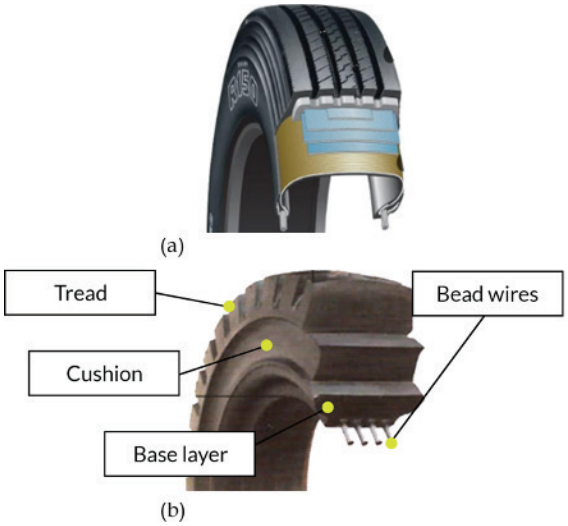

Figure 1 - Cross sections: (a) pneumatic tire and (b) solid tire

In numerical analysis, the majority of existing literature has concentrated on the examination of pneumatic tires [1, 2]. Limited research has been conducted to explore the static and dynamic properties of solid resilient tires. Suripa and Chaikittiratana (2008) [3] examined the strain energy density and stress distribution in solid tires under static conditions utilizing simplified 3D finite element solid models. Their findings indicated that the maximum strain energy was located in the cushion layer of the solid tire.

Dechwayukul et al. (2010) [4] carried out laboratory experiments to assess the durability and service life of solid tires. In a separate study, Phromjan and Suvanjumrat (2018) [5, 6] developed a comprehensive 3D finite element model to examine the deformation and stress distribution in solid tires under various static load conditions. Their findings revealed significant stress in the base layer of the solid tire. Additionally, they conducted laboratory experiments to compare the contact forces and vibration responses of rolling solid tires with those of pneumatic tires at different rolling speeds. The study found that solid tires exhibited higher contact forces and vibration levels compared to pneumatic tires.

Research on solid tires are relatively limited, and there is a significant gap in understanding how variations in layer materials and bead wire percentages influence key performance metrics. No studies have specifically examined the effects of these modifications on vertical displacement, horizontal displacement, and contact area. Understanding these relationships is crucial for optimizing solid tire design, improving durability, and enhancing performance in various applications. This research aims to address this gap by systematically analysing how material composition and bead wire distribution impact the structural behaviour of solid tires.

Additionally, this research explores the theoretical and mathematical formulations of constitutive relationships for filled vulcanized rubber. Furthermore, the study presents the methodology for identifying the most suitable constitutive relationship for a specific carbon black-filled rubber compound, a material extensively used in the industrial solid tire industry. Finally, this study focuses on the development of a 3D static finite element model for an industrial solid resilient tire, using the selected hyper-elastic material model. Given these factors, the main objective of this study is to understand how changes in layer thickness and the percentage of bead wire affect the static performance of solid tires. A numerical approach will be used to find the best configurations for better performance.

2. Hyper-elastic Material Models

In the context of finite element analysis for tire simulation, hyper-elastic material models play a crucial role due to their ability to accurately represent the behaviour of rubber like materials which are prevalent in tires. The most notable characteristic of rubbers is their ability to undergo significant deformation under relatively small loads while returning to their original shape with minimal permanent deformation once the load is removed [7].

Hyper-elastic materials are characterized by their capacity to undergo significant elastic deformations and return to their original shape upon unloading, making them ideal for modelling the complex, non-linear stress-strain relationships observed in tires. Accurate material modelling is essential for predicting tire performance, durability, and safety. Common hyper-elastic models, such as the Neo-Hookean, Mooney-Rivlin, and Ogden models, are widely used in finite element analysis to capture the material response under various loading conditions. These models require precise experimental data for calibration to ensure that the simulations accurately reflect the physical properties of the tire materials. By employing

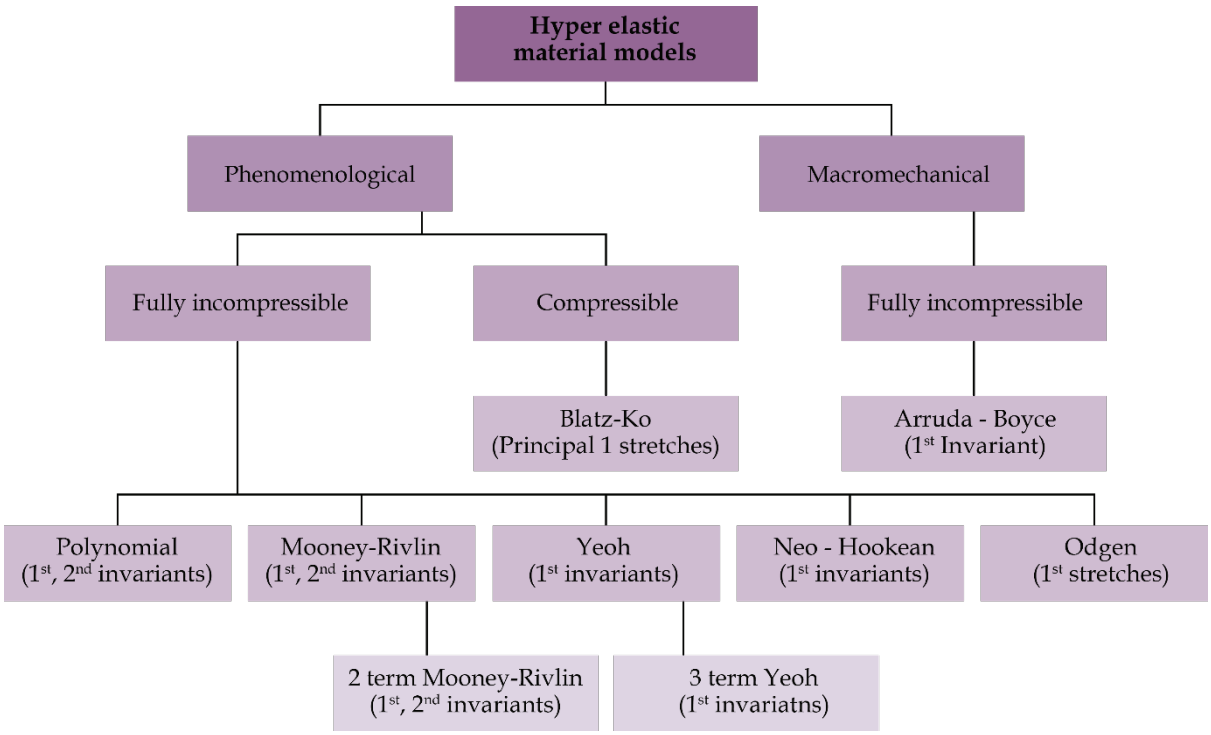

Figure 2 – Hyper-elastic model classification

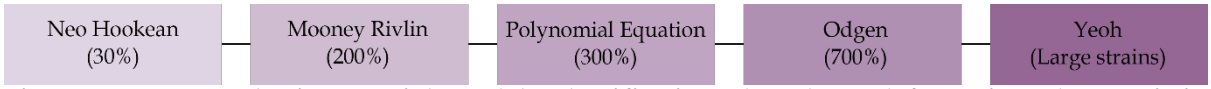

Figure 3 - Hyper-elastic material models classifications based on deformation characteristics (strain - (%))

hyper-elastic material models, engineers can better predict how tires will perform under different conditions, ultimately leading to safer and more reliable tire designs.

Hyper-elastic material models can be broadly classified into two categories, as shown in Figure 2. The first category encompasses phenomenological models, which are derived from the principles of continuum mechanics. In these models, material constants are determined through a curve fitting approach. The second category includes micro-mechanical models, which are based on the microstructure of the material. These models obtain material constants through specific material tests used to capture the detailed characteristics of the material [8, 9].

Material models can also be categorized based on deformation characteristics, as illustrated in Figure 3. Several researchers have developed their own strain-energy density functions, particularly for large strain scenarios [10, 11, 12, 13]. In addition to that, they have validated these models experimentally [5, 8, 14, 15, 16]. Despite the numerous constitutive models proposed to describe the elastic response of elastomers, only a limited research effectively captures the complete behaviour of the material under various loading conditions, including uniaxial, biaxial tension and compression, and planar tests [14]. The most accurate models are generally those that describe the comprehensive behaviour of rubber-like materials using a minimal number of experimentally determined material parameters [14].

Considering the above mentioned points, Mooney developed a general strain-energy function founded on three key assumptions [12]: (1) material exhibits isotropy, (2) volume change and hysteresis effects are negligible, and (3) shear stress is proportional to traction. This function aims to describe the stress-strain behaviour through both the statistical mechanics of rubber elasticity and continuum mechanics theories based on invariants or stretches [10].

The stress-strain relationship for a hyper-elastic, isotropic rubber-like material is derived from the strain-energy density function as shown in Eq. (1). This function, denoted as W, represents the strain energy stored in the material per unit reference volume. The formulation of this relationship can be simplified using an approach comparable to Hooke's law.

$$S_{ij} = \frac{\partial W}{\partial E_{ij}} \qquad \ldots(1)$$

In the above equation, S_{ij} represents the components of the second Piola-Kirchhoff stress tensor, while E_{ij} denotes the components of the Lagrangian strain tensor. The strain-energy density function (W) can be mathematically described using finite deformation quantities, such as Green's strain, the invariants of the Cauchy-Green deformation tensor, or principal stretch ratios as frame-invariant strain measures. Specifically, W can be expressed as a function of the invariants I_1, I_2 and I_3. Additionally, W can be decomposed into a deviatoric term (W_d) and a volumetric term (W_b), resulting in the formulation $W = W_d(I_1 + I_2) + W_b(J_{el})$.

In continuum mechanics, the strain-energy density function depends on the stretch via the first, second, and third invariants I_1, I_2 and I_3. These invariants are defined as follows: $I_1 = \lambda_1^2 + \lambda_2^2 + \lambda_3^2$, $I_2 = \lambda_1^2\lambda_2^2 + \lambda_2^2\lambda_3^2 + \lambda_3^2\lambda_1^2$ and $I_3 = \lambda_1^2\lambda_2^2\lambda_3^2$ of the stretch tensor [10]. The stretch tensor depends on the strain through the principal stretches λ_1, λ_2 *and* λ_3 which fully specify the state of strain at each material element relative to a given reference configuration [15]. For incompressible materials, the relationship $\lambda_1\lambda_2\lambda_3 = 1$ holds. For rubber-like materials, the Poisson's ratio (ν) is approximately 0.5 [17]. In Eq. (2), K_0 represents the initial bulk modulus and μ_o the initial shear modulus.

$$\nu = \frac{\left(\frac{3K_0}{\mu_0} - 2\right)}{\left(\frac{6K_0}{\mu_0} + 2\right)} \qquad \ldots(2)$$

The polynomial model equation is formulated to include both deviatoric and volumetric terms, as shown in Eq. (3).

$$\mathrm{W} = \sum_{i=0}^{n} C_{ij}(\overline{I_1 - 3})^i(\overline{I_2 - 3})^j + \sum_{i=1}^{N} \frac{1}{D_i}(J_{el} - 1) \qquad \ldots(3)$$

In this context, C_{ij} is a material constant that governs the shear behavior and can be determined from uniaxial, biaxial, and planar tests. D_i is the material constant that controls bulk compressibility, with the initial bulk modulus $K_0 = \frac{2}{D_1}$ For fully incompressible rubber, D_i is set to zero. This constant is estimated from volumetric tests, and J_{el} represents the elastic volume ratio.

Several factors influence the properties of elastomers. These include static preload, which causes a compressive permanent set in a segment, and periodic deformation, which leads to hysteresis behaviour and heat generation [18]. The stress-strain behaviour of elastomers exhibits the Mullins effect, which is dependent on the maximum deformation previously experienced by the material. Other factors include the Payne effect, creep, relaxation, and losses due to sinusoidal input [19, 20]. This behaviour results in configurational entropy changes during stretching and recoiling [10]. The entropy change during the stretching of rubber is calculated using statistical methods, disregarding intermolecular attractions.

Various strain energy potentials are available for modelling nearly incompressible isotropic elastomers as shown in Table 1. These include the Mooney-Rivlin, Neo-Hookean, Yeoh, Ogden, Arruda-Boyce, Marlow, Polynomial, Reduced Polynomial, and Van der Waals forms. Based on the literature, the four most popular models were selected for their applicability.

3. Numerical Modelling of Solid Resilient Tires

Finite Element Analysis is applied as a method that uses mathematical approximations to replicate geometry, load scenarios, interactions, and boundary conditions. In finite element analysis (FEA), the physical problem is discretized into a mesh of small finite elements with unknown nodal values. The finite element method (FEM) is implemented through computational algorithms to solve for these unknowns, for the determination of stresses, displacements, and other relevant parameters based on the material properties, applied loads, and boundary conditions.

A reliable prediction of tire performance needs the development of a robust and detailed numerical 3D tire model. Such a model is fundamental for capturing the complex interactions between the tire's structure and its operating conditions. To achieve this level of accuracy, it is essential to have an extensive and high-quality set of material test data, which includes the mechanical properties and behaviours of the materials used in tire construction. In addition, the geometric details of the tire, such as tread patterns, sidewall dimensions, and internal structures, must be precisely represented in numerical model. Together, these elements ensure that the numerical model can simulate the tire's performance under various loads, speeds, and

environmental conditions with a high degree of fidelity.

In this research, the advanced software *ABAQUS* was used for FE analysis. The FE simulation was conducted by following the three primary steps: pre-processing, model solving, and post-processing [25]. The steps followed to develop the static numerical model of the tire are shown in Figure 4.

Table 1 - Constitutive models for hyper-elastic material

Model	Remarks	Governing equation
Mooney Rivlin [9, 13, 21]	• Two-parameter phenomenological model • Fits well for moderately large strains about 100%, to 200% • Used for the bodies of ideal highly elastic materials which are incompressible and isotropic in their undeformed state • This model does not obey the filled rubber • The most used form is the two-term Mooney Rivlin model	$W = C_{10}(\bar{I}_1 - 3) + C_{01}(\bar{I}_2 - 3) + \frac{1}{D_1}(J_{el} - 1)^2$ I_1, I_2 = The principal invariants of the deviatoric Cauchy-Green deformation tensor C_{ij}, D_i = Temperature dependent material constants J_{el} = Elastic volume ratio
Neo-Hookean [17, 22, 23]	• A reduced form of Mooney Rivlin form with $C_{01} = 0$ • Can be used when material data is insufficient • Makes good approximation at relatively small strains (30%) at the initial linear range	$W = C_{10}(\bar{I}_1 - 3) + \frac{1}{D_1}(J_{el} - 1)^2$ I_1 = The principal invariants of the deviatoric Cauchy-Green deformation tensor C_{ij}, D_i = Temperature dependent material constants J_{el} = Elastic volume ratio
Ogden [22, 24]	• This is based on principal stretch ratios • This is a power series with added extra terms for additional degrees of freedom which allows the regression analysis in fitting stress-strain data • Fits for large deformations up to 700% • A good agreement in experimental data for unfilled rubber	$W = \sum_{i=1}^{N} \frac{2\mu_i}{\alpha_i^2}(\bar{\lambda}_1^{\alpha_i} + \bar{\lambda}_2^{\alpha_i} + \bar{\lambda}_3^{\alpha_i} - 3) + \sum_{i=1}^{N} \frac{1}{D_1}(J_{el} - 1)^2$ $\bar{\lambda}_1$ = Deviatoric principal stretch μ_1, α_1, D_i = Temperature dependent material coefficients
Arruda-Boyce [10]	• Statical mechanical model • It is based on the molecular 8-chain network, based on the representative volume (hexahedron) element from the center to the corners • Two-parameter shear model fits well with limited test data	$W = \mu \sum_{i=1}^{5} \frac{C_i}{\lambda_m^{2i-2}}(\bar{\lambda}_1^i - 3^i) + \frac{1}{D_i}\left(\frac{J_{el}^2 - 1}{2} - \ln(J_{el})\right)$ $\bar{\lambda}_1$ = Deviatoric principal stretches C_{ij}, D_i = Temperature dependent material constants $\mu = 2(C_{10} + C_{01})$ = initial shear modulus

The numerical model in *ABAQUS* comprises five components as shown in Figure 5, the tread, cushion layer, base layer, bead wires, and road. These layers are made of three different rubber compounds with distinct properties. The base layer is the hardest of all and is embedded with bead reinforcements. Its hardness is achieved using a special non-thermoplastic rubber compound, which prevents softening over time. The steel bead wires provide strength while maintaining the rubber's flexibility. The inner layer of the base layer is designed to prevent the tire from rotating on the rim, while the cushion layer helps maintain balance. The resilience and hardness of the middle part of the cushion layer ensure low heat build-up and provide better comfort. The tread layer prevents sidewall tears and ensures minimal wear, performing well on rough terrains. Additionally, it exhibits high tensile and tear resistance properties to minimize chipping and fragmenting.

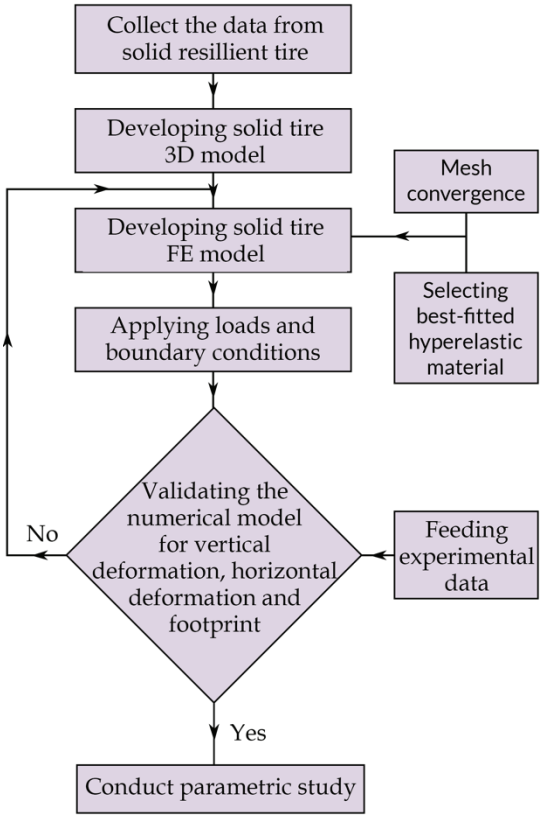

Figure 4 - Flow chart of FE model development and validation

The interactions between each component are presented in Table 2 and Figure 6. The boundary conditions for the tire are defined such that the road is fixed to prevent displacements and transformations in all six degrees of freedom. The boundary condition of the loading is only allowed to translate in the downward direction.

The mesh used in this study is based on a 3D stress element configuration. Eight-node brick elements (C3D8RH) were used for modelling the cushion layer, base, and bead wires. The tread layer, as shown in Figure 7, was modelled using 10-node modified quadratic tetrahedron elements (C3D10MH), hybridized with linear pressure.

Table 2 - The interaction properties between different layers

Interaction	Master	Slave	Type
Road-Tire	Road	Tire	Surface to Surface $\mu = 0.7$
Cushion-Tire	Tread	Cushion	Tie
Base-Cushion	Base	Cushion	Tie

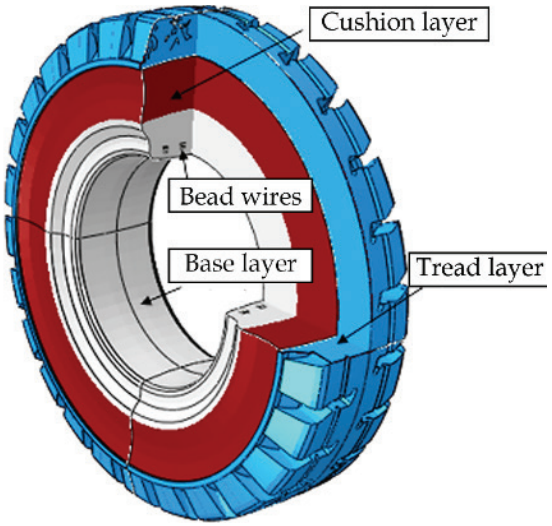

Figure 5 - Numerical model of solid tire component with different layers

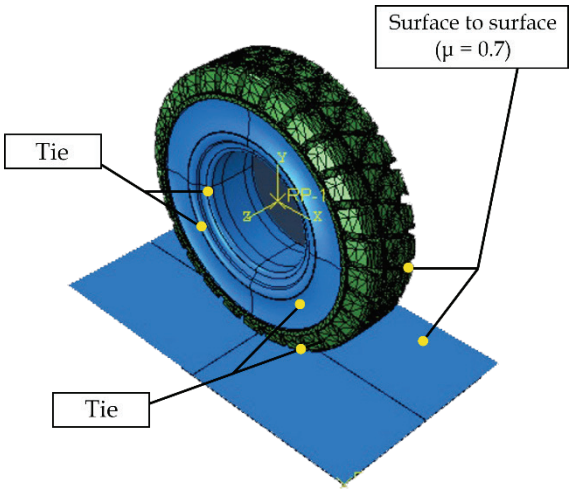

Figure 6 - Interaction between each layer of solid tire FE model

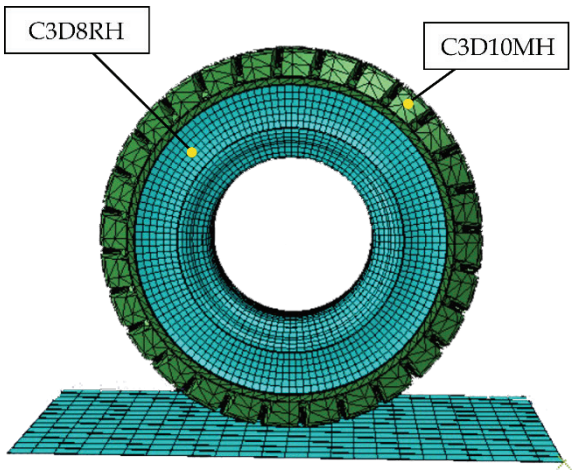

Figure 7 - Types of mesh elements in solid tire FE model

3.1 Selection of an Appropriate Material Model for FE Simulation

Determining the optimal constitutive material model to assess the hyper-elastic behaviour of rubber compounds is essential. Curve fitting is the method used to adjust the parameters of a model function so that the fitted curve closely aligns with the measured data. Accurate material testing data is crucial to effectively fit the large strain response of rubber and elastomer materials. The uniaxial tests are straightforward to perform and widely understood [26]. However, relying solely on uniaxial data does not yield a reliable set of coefficients for material models [27]. At least two material tests, including uniaxial tension or compression, biaxial tension or compression, planar shear, and volumetric tests, are required for a robust evaluation between test data and constitutive models [14, 20].

The curve fitting process for hyper-elastic material models involves four steps. First, the stress-strain curves must be revised and adapted using test data, with the least-squares method used to determine the quality of curve fitting for the data points. Second, a constitutive equation (material model) must be selected, and the curves for the mostly used hyper-elastic material models are plotted. Third, error calculations are performed to compare the curves against test data using three selected statistical indexes: Mean Absolute Percentage Error (MAPE), Mean Absolute Deviation (MAD), and Mean Squared Deviation (MSD), as shown in Eqs. (4), (5) and (6) respectively. In these equations, y_t represents stress values of the test data, while $\hat{y}$ represents the stress values predicted by the selected constitutive model. The final step is to conduct both a qualitative and quantitative comparison of the resulting curve of the selected material model with the test data.

$$MAPE = \frac{\sum_{t=1}^{n}\left|\frac{y_t - \hat{y}}{y_t}\right|}{n} 100\% \quad \ldots(4)$$

$$MAD = \frac{\sum_{t=1}^{n}|y_t - \hat{y}|}{n} \quad \ldots(5)$$

$$MSD = \frac{\sum_{t=1}^{n}|y_t - \hat{y}|^2}{n} \quad \ldots(6)$$

In this study, uniaxial tensile test data and planar shear data are used for analysis. The strain-energy density values of the material are derived using specific equation formulations for each model, optimizing the material parameters based on the provided test data. The Yeoh model is commonly used by researchers when limited test data is available [9, 16]. All hyper-elastic models rely on fitted coefficients. Among the obtained hyper-elastic curves, the Ogden model exhibits instability for the available test data, whereas the Arruda-Boyce, Neo-Hookean, and Yeoh models remain stable. Statistical indexes for these four material models are summarized in Table 4.

The error measurements indicate that the Yeoh material model yields the lowest values for these statistical indexes, establishing it as the best-fitted material model for further analysis in this study. Hence, in the numerical model, the tread layer, cushion layer, and base layer are modelled as Yeoh material model, as shown in Table 3. The bead wires are designed as a steel material. The density of the steel material was measured to be 7688 kgm^{-3}. The Young's modulus was determined to be 200 GPa, and the Poisson's ratio was found to be 0.3. The coefficients for the hyper-elastic materials are determined using the best-fitted hyper-elastic model based on uniaxial test data.

Table 3 - Material properties of each layer of the tire

Layer	Density (kg/m^3)	Poisson's Ratio	Hyper-elastic Model
Tread	1150	0.49	Yeoh
Base	1220	0.49	Yeoh
Cushion	1130	0.49	Yeoh

3.2 Numerical Convergence Study

The variation of vertical displacement (U2) as shown in Figure 8 and maximum stresses on the reinforcement were analysed with respect to number of elements for the mesh convergence study. The results showed that the converged number of elements are 130,000, as illustrated in Figure 9 and Figure 10. Following the mesh convergence study, the element sizes for the selected meshes are presented in Table 5.

Table 4 - Statistical indexes of selected constitutive models

Layers	Base			Cushion			Tread		
Statistical index	Arruda	Neo	Yeoh	Arruda	Neo	Yeoh	Arruda	Neo	Yeoh
MAPE	22.26	22.26	4.84	100	32.92	4.61	17.6	34.99	7.55
MAD	0.96	0.96	0.28	9.34	3.47	0.17	1.53	3.74	0.36
MSD	1.2	1.2	0.11	129.54	22.61	0.04	4.41	26.95	0.19

Table 5 - Element sizes of the converged meshes

Layer	Element Size(mm)
Base	9
Bead	10
Cushion	9
Tread	-

3.3 Validation of Solid Tire Model

The test data gathered from the industrial experiment was used to validate the model. A quasi-static load, increasing from 0 to 2800 N, was applied to the top surface of the tire in the U2 direction, as shown in Figure 11. Then, the vertical displacement (U2), horizontal displacement (U3) and contact areas were obtained. To determine the experimental contact area, the contact patch was imported into AutoCAD, where the area was calculated. Figure 12 shows the obtained contact patch for the 2800 N vertical load.

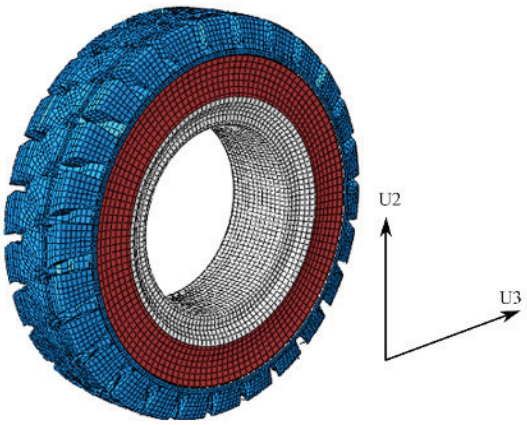

Figure 8 – U2 and U3 direction on solid tire

The developed three-dimensional finite element (FE) model of solid tires provides a reliable prediction for the static analysis under a vertical load of 0 N to 2800 N. The key parameters obtained from the static analysis include strain energy density, von Mises stress, vertical displacement (U2), horizontal displacement (U3), and maximum stress. Figures 13 and 14 illustrate the distribution of von Mises stress and vertical displacement for the solid tire under the applied load, respectively.

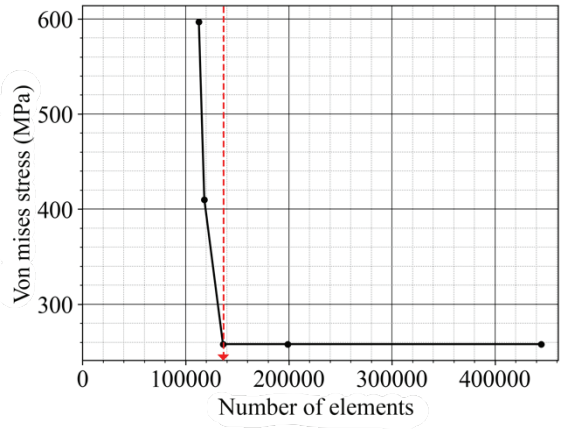

Figure 9 - Variation of maximum stress on reinforcements with number of elements

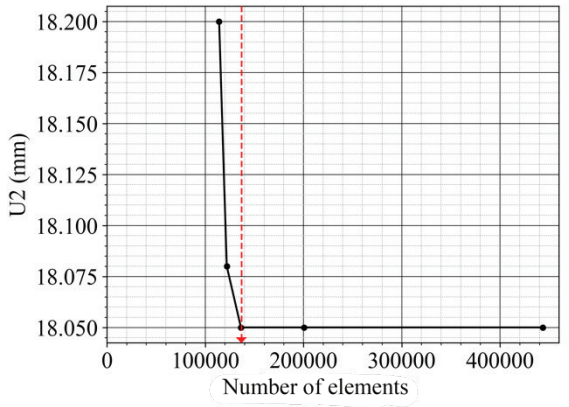

Figure 10 - Variation of vertical displacement with load with number of elements

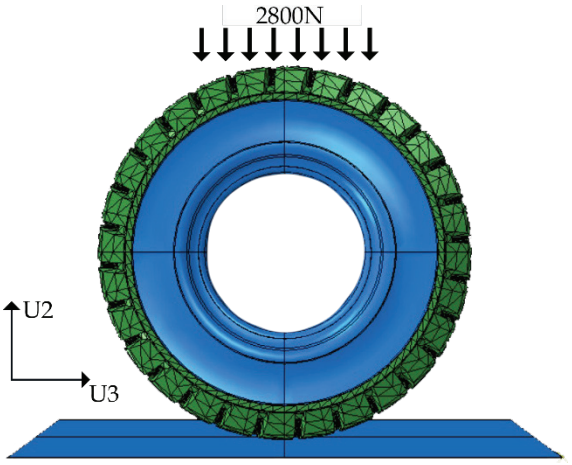

Figure 11 - 2800N load to U2 direction for static analysis

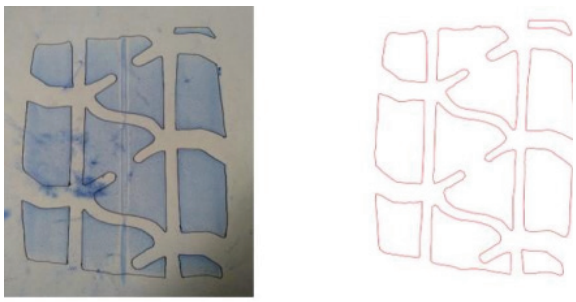

(a) (b)

Figure 12 - Contact patches for 2800N: (a) experimental and (b) CAD drawing

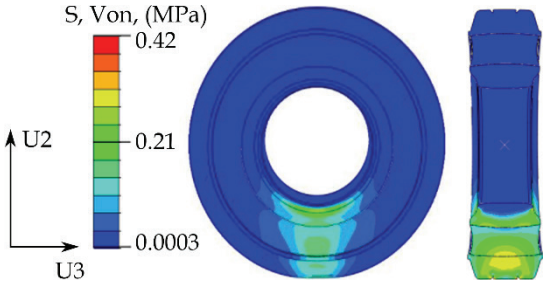

Figure 13 - von Mises stress distribution of rubber at 2800N

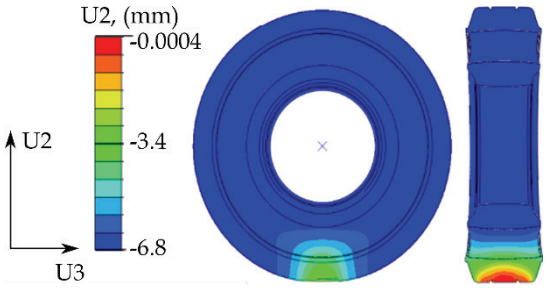

Figure 14 - Displacement distribution on vertical direction (U2) at 2800N

A 2800 N load was gradually applied to both the experimental and numerical setups, starting from zero load. Figures 15, 16 and 17 illustrate the distribution of vertical displacement, horizontal displacement and contact area for the solid tire under the applied loading, respectively.

Additionally, MAPE, MAD, and MSDE values were calculated using the numerical and experimental values of vertical displacement, horizontal displacement, and contact area, as shown in Table 6. Since these values are below 5%, it can be said that the numerical model is in good agreement with the experimental results. Next, this validated FE model is used to conduct the two parametric studies aimed at evaluating the static performance of solid tires.

4. Static Performances of Solid Resilient Tire

The main objective of this study is to evaluate the static performance of solid tires by varying different parameters. In this research, the following two key parameters are varied: (1) material properties of the solid tire layers, and (2) percentage of steel reinforcement.

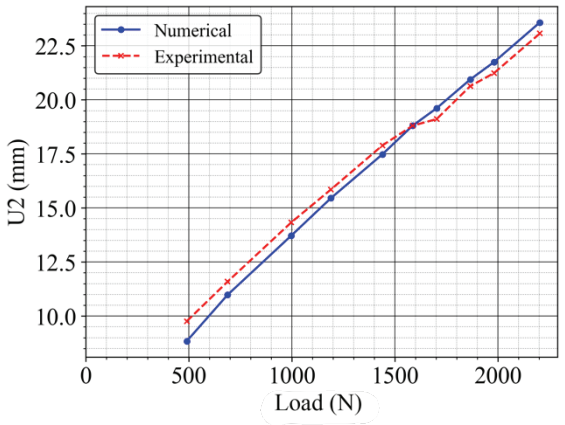

Figure 15 - Validation of vertical displacement (U2) with load

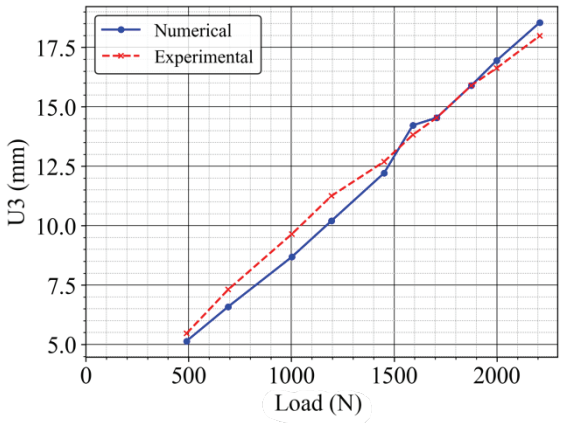

Figure 16 - Validation of horizontal displacement (U3) with load

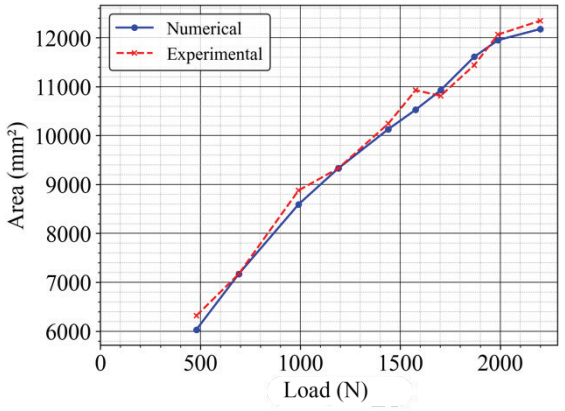

Figure 17 - Validation of contact area with load

Table 6 - Statistical indices for validation

Parameters	MAPE	MAD	MSDE
U2	4.32	0.39	0.22
U3	2.81	0.39	0.20
Contact area	1.45	1.34	1.79

4.1 Varying the Material Properties of the Layers

Solid tires consist of three distinct layers: base, cushion, and tread. Each layer is made from rubber materials with different properties. The base material is the hardest and most expensive, while the cushion is the softest and least expensive. The tread material is softer than the base but harder than the cushion, making it more economical than the cushion but more expensive than the base.

4.1.1 Setup of parametric study

To evaluate tire performance, upper limit and lower limit are considered: lower limit is using the base material for all layers (hardest case), and upper limit is using the cushion material for all layers (softest case). The variation in material properties in tire are detailed in Figure 18 and Table 7.

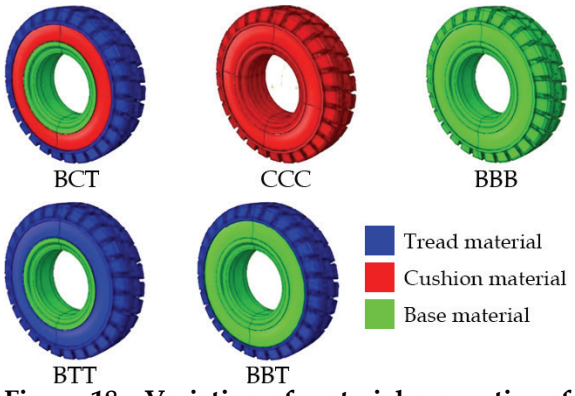

Figure 18 - Variation of material properties of tire layers (B: Base layer, C: Cushion layer, T: Tread layer)

4.1.2 Results and Discussion

In the parametric study of varying the tire layer material properties, the CCC model showed the maximum displacement, while the BBB model showed the lowest displacement. As expected, the BBT and BTT models showed lower displacements (horizontal and vertical) compared to the original BCT model. The results indicate that displacement decreases as the material hardness increases. The displacement distribution in the vertical and horizontal directions is shown in Figure 19 and Figure 20, respectively.

When vertical and horizontal displacement decreases as material gets harder, the reduction in the contact area also can be observed. The CCC model has the largest contact area, therefore, only the BCT, BBT, and BTT models were considered for contact area variation. The variation in contact area is shown in Figure 21.

The percentage variations from the original BCT model at the 2800N loading case for vertical displacements, horizontal displacements, and contact area are presented in Table 8.

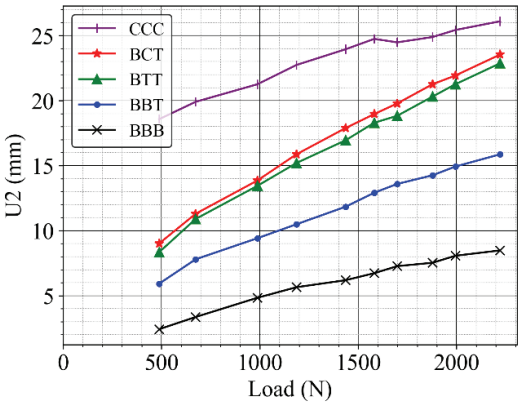

Figure 19 - Variation of vertical displacement with load

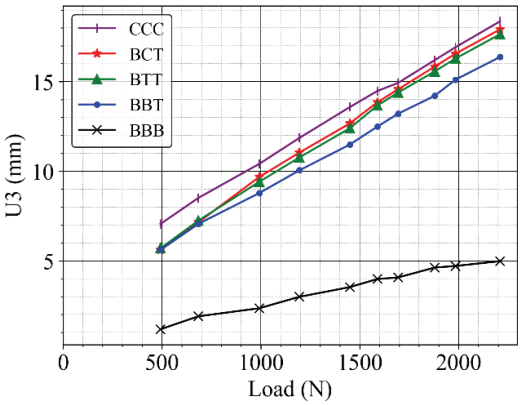

Figure 20 - Variation of horizontal displacement with load

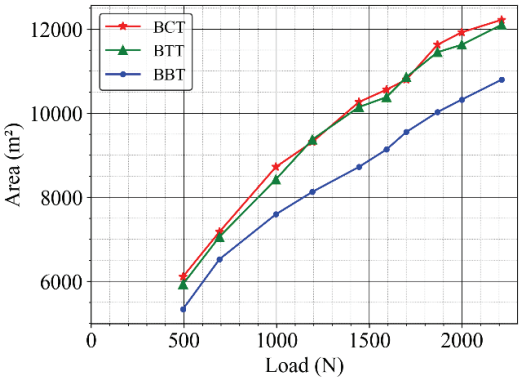

Figure 21 - Variation of contact area with load

Table 8 – Percentage variation of the horizontal (d_x), vertical displacement (d_y) and contact area (A)

Tire Layer Structure	Percentage (%)		
	d_y	d_x	A
CCC	66%	08%	NA
BBT	-33%	-08%	-13%
BTT	-04%	-02%	-2%
BBB	-41%	-73%	NA

Table 7 - Tire layer's material variation

Part	Material Property				
	Original	Upper limit	Lower limit	Case 1	Case 2
Base	Base (B)	Cushion (C)	Base (B)	Base (B)	Base (B)
Cushion	Cushion (C)	Cushion (C)	Base (B)	Tread (T)	Base (B)
Tread	Tread (T)	Cushion (C)	Base (B)	Tread (T)	Tread(T)

4.2 Varying the Percentage of Reinforcement

In this parametric study investigating the effects of varying reinforcement percentages in tires, the original tire's reinforcement level is considered as 100% reinforcement.

4.2.1 Setup of parametric study

Five conditions were evaluated corresponding to reinforcement percentages of 0%, 25%, 50%, 75%, and 100% of the original tire as shown in Figure 22. All reinforcements were centrally aligned for consistency. The material properties of the original tire were retained throughout the parametric study. The analysis focused on the variation of horizontal and vertical displacements, the stress distribution in both reinforcements and rubber components, and the changes in contact area under applied load.

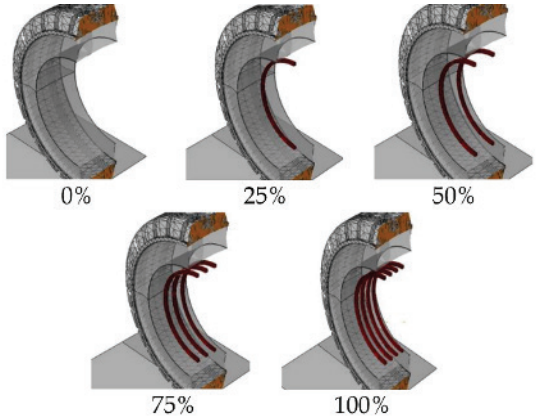

Figure 22 - Alignment of reinforcement in the models

4.2.2 Results and Discussion

In the analysis of the variation of vertical and horizontal displacements under different loading conditions, the results indicate that at lower load levels, there is no significant observable variation. However, as the loading increases, a greater variation in displacement becomes apparent. This trend may be attributed to the consistency in material properties throughout the experiment, which limits noticeable variations at lower loads. The vertical and horizontal displacement variations are illustrated in Figures 23 and 24, respectively.

The maximum stress in the reinforcements varies with the percentage of reinforcement. A reduction in maximum stress is generally expected as the percentage of reinforcement increases. However, in this case, the maximum stress at 50% reinforcement is observed to be higher than that at 25% reinforcement. This reduction could be due to the alignment of the reinforcements. Further investigation could suggest to assess the influence of reinforcement alignment on stress distribution. Other observed conditions followed the expected trends. The maximum stress in the rubber material did not show significant variation with changes in reinforcement percentage. The variation in maximum stress on the reinforcements and the rubber is illustrated in Figures 25 and 26, respectively.

The variation in contact area with different reinforcement percentages did not have significant changes. Therefore, further studies are recommended to explore the influence of reinforcement on the contact area in greater detail. The variation of contact area with load is shown in Figure 27.

The percentage differences for various cases compared to the original 100% reinforcement model, including vertical displacements, horizontal displacements, contact area, and stresses on the rubber and reinforcement, are presented in Table 9.

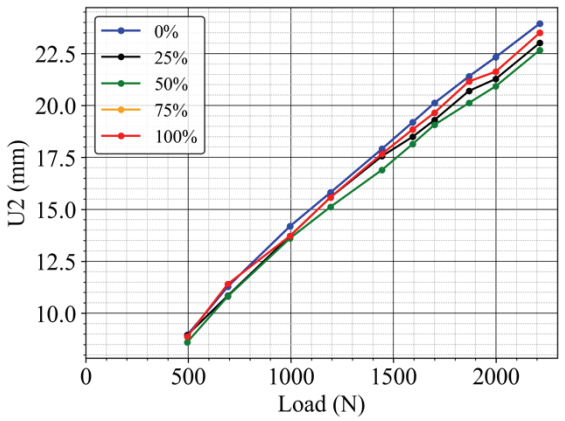

Figure 23 - Variation of vertical displacement with load at different percentages of bead wires

Table 9 - The percentage variation of 0%, 25%, 50%, 75% of reinforcement configurations

Reinforcement percentage in the solid tire (%)	Variation percentage				
	Vertical Displacement	Horizontal Displacement	Contact area	von Mises stress on rubber	von Mises stress on reinforcement
0%	1.864%	0.678%	0.062%	1.219%	NA
25%	1.580%	2.757%	1.610%	4.516%	41.954%
50%	3.468%	2.072%	1.606%	5.286%	44.723%
75%	0.001%	0.001%	0.001%	0.001%	11%

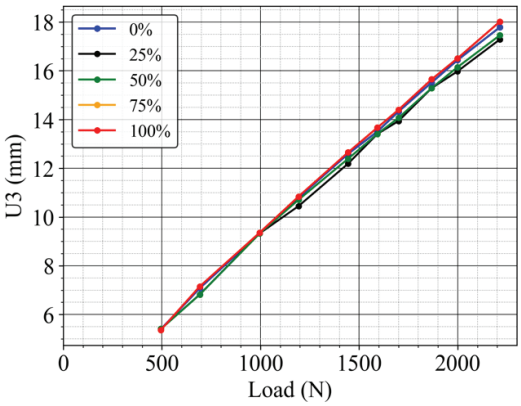

Figure 24 - Variation of horizontal displacement with load at different percentages of bead wires

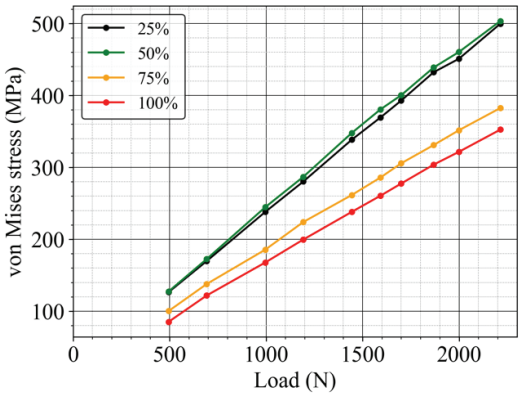

Figure 25 - Variation of maximum von Mises stress on reinforcement with load at different percentages of bead wires

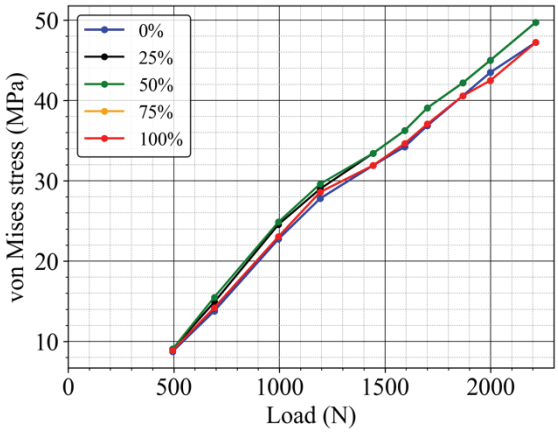

Figure 26 - Variation of maximum von Mises stress on rubber with load at different percentages of bead wires

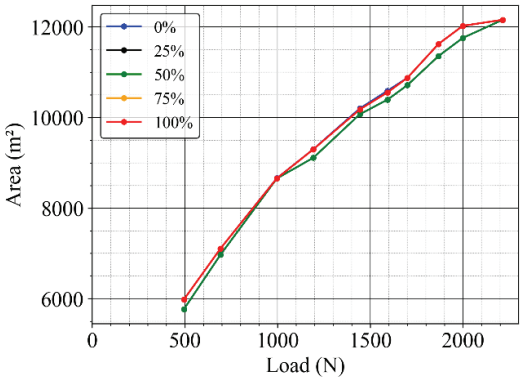

Figure 27 - Variation of contact area with load at different percentages of bead wires

5. Conclusion

This research investigates the static performance of solid tires with respect to changes in layer thickness and bead wire percentage using a numerical approach. Selecting the most suitable hyperelastic material model for rubber-like materials, based on provided experimental test data, is crucial for obtaining a well-validated numerical model. In this study, a curve-fitting approach with three statistical indices—MAPE, MAD, and MSD—was employed to identify the best hyperelastic material model for the target solid tire layers.

Subsequently, the validated FE model was used to evaluate the static performance of the solid tire by varying key parameters such as layer properties and reinforcement percentages. This approach aims to predict the performance of the solid tire under static loading conditions and provide insights into the influence of these parameters on overall behavior. The study led to the following conclusions and recommendations:

- Based on uniaxial and planar shear test data, the curve-fitting method and statistical indices (MAPE, MAD, and MSD) were used to determine the most suitable material model from the four commonly used hyperelastic models (Mooney Rivlin, Neo-Hookean, Ogden, Arruda-Boyce) identified in the literature. Results show that the Yeoh hyperelastic material model had the

closest fit to the experimental data, making it the most appropriate choice for this study. The accuracy of the chosen model can be improved by incorporating additional test data during the selection process.

- The first parametric study was conducted by altering the material properties of the solid tire layers. The lower and upper bounds for vertical and horizontal deflection were observed when the solid tire was composed entirely of Base (BBB) material and Cushion (CCC) material, respectively. The percentage differences for the BBB case in vertical deflection, and horizontal deflection compared to the original tire model are -41 %and -73 %, respectively. For the CCC case, these values are 66 % and 08 %, respectively. It is evident that adjusting the layer thickness is necessary to achieve the desired comfort level of the solid tire. Further research is recommended to determine the required thickness for each layer to meet specific comfort criteria.
- The second parametric analysis involved varying the reinforcement percentages of the tire in a center-aligned configuration. Five reinforcement configurations were tested: 0%, 25%, 50%, 75%, and 100%. The results indicate that reinforcement percentage has minimal impact on the static performance of the solid tire. However, it is recommended to conduct dynamic simulations to assess the effect on dynamic performance, as reinforcements play a key role in energy dissipation under high-impact forces.

Acknowledgement

The authors would like to give their acknowledgement for licensed applications of the *ABAQUS* package facilitated by the Finite Element Analysis and Simulation Centre, Rubber Research Institute of SriLanka, Ratmalana

References

1. Han, M. J., Lee, C. H., Park, T. W., Kim, Y. S., Shin, K. D., & Sim, K. S., 'Cleat Impact Analysis of a Multi-body Quarter Vehicle System with Finite Element Models', *Int. J. Mech. Eng. Robot. Res.*, Vol. 8, No. 6, 2019, pp. 880–884.

2. Azizi, Y., 'Measurement Methods of Tire/Road Noise', *Automotive Tire Noise and Vibrations*, Elsevier, 2020, pp. 65–90.

3. Suripa, U., Chaikittiratana, A., 'Finite Element Stress and Strain Analysis of a Solid Tyre', *J. Achiev. Mater. Manuf. Eng.*, Vol. 31, No. 2, 2008, pp. 576–579.

4. Dechwayukul, C., Kao-ien, W., Chetpattananondh, K., & Thongruang, W., 'Measuring Service Life and Evaluating The Quality of Solid Tires', *Sonklanakarin J. Sci. Technol.*, Vol. 32, No. 4, 2010, p. 387.

5. Phromjan, J., Suvanjumrat, C., 'A Suitable Constitutive Model for Solid Tire Analysis Under Quasi-Static Loads Using Finite Element Method', *Eng. J.*, Vol. 22, No. 2, 2018, pp. 141–155.

6. Phromjan, J., Suvanjumrat, C., 'Vibration Effect of Two Different Tires on Baggage Towing Tractors', *J. Mech. Sci. Technol.*, Vol. 32, 2018, pp. 1539–1548.

7. Brinson, H. F., Brinson, L. C., 'Polymer Engineering Science and Viscoelasticity', 2008.

8. Rackl M., 'Material Testing and Hyperelastic Material Model Curve Fitting for Ogden', *Polynomial Yeoh Models*, 2015.

9. Shahzad, M., Kamran, A., Siddiqui, M. Z., & Farhan, M., 'Mechanical Characterization and FE Modelling of a Hyperelastic Material', *Mater. Res.*, Vol. 18, No. 5, 2015, pp. 918–924.

10. Boyce, M. C., Arruda, E. M., 'Constitutive Models of Rubber Elasticity: a Review', *Rubber Chem. Technol.*, Vol. 73, No. 3, 2000, pp. 504–523.

11. Ogden, R. W., 'Large Deformation Isotropic Elasticity–on the Correlation of Theory and Experiment for Incompressible Rubberlike Solids', *Proc. R. Soc. Lond. Math. Phys. Sci.*, Vol. 326, No. 1567, 1972, pp. 565–584.

12. Mooney, M., 'A Theory of Large Elastic Deformation', *J. Appl. Phys.*, Vol. 11, No. 9, 1940, pp. 582–592.

13. Yeoh, O. H., 'Characterization of Elastic Properties of Carbon-Black-Filled Rubber Vulcanizates', *Rubber Chem. Technol.*, Vol. 63, No. 5, 1990, pp. 792–805.

14. Marckmann, G., Verron, E., 'Comparison of Hyperelastic Models for Rubber-Like Materials', *Rubber Chem. Technol.*, Vol. 79, No. 5, 2006, pp. 835–858.

15. Hossain, M., Denzer, R., Possart, G., & Steinmann, P., 'On Phenomenological and Micro-Mechanical Models in Finite Elasticity and Viscoelasticity for Rubber-Like Materials', *Proceedings in Applied Mathematics and Mechanics*, 2007, pp. 4060051–4060052.

16. Huri, D., Mankovits, T., 'Comparison of the Material Models in Rubber Finite Element Analysis', *IOP Conference Series: Materials Science and Engineering*, 2018, p. 012018.

17. Crocker, L., Duncan, B., Urquhart, J., Hughes, R., & Olusanya, A., 'The Application of Rubber Material Models to Analyse Flexible Adhesive Joints', *Proc. Adhes.*, Vol. 99, 2007.

18. Marvalova, B., 'Viscoelastic Properties of Filled Rubber. Experimental Observations and Material Modelling', *Eng. Mech.*, Vol. 14, No. 1/2, 2007, pp. 81–89.

19. Vijayaram, T. R., 'A Technical Review on Rubber', *Int. J. Des. Manuf. Technol.*, Vol. 3, No. 1, 2009, pp. 25–37.

20. Jerrams, S., Murphy, N., *Constitutive models for rubber VII*. CRC Press, 2011.

21. Rivlin, R. S., Saunders, D., 'Large Elastic Deformations of Isotropic Materials VII. Experiments on the Deformation of Rubber', *Philos. Trans. R. Soc. Lond. Ser. Math. Phys. Sci.*, Vol. 243, No. 865, 1951, pp. 251–288.

22. Yeoh, O. H., Fleming, P., 'A New Attempt to Reconcile the Statistical and Phenomenological Theories of Rubber Elasticity', *J. Polym. Sci. Part B Polym. Phys.*, Vol. 35, No. 12, 1997, pp. 1919–1931.

23. Kim, B., 'A Comparison Among Neo-Hookean Model, Mooney-Rivlin Model, and Ogden Model for Chloroprene Rubber', *Int. J. Precis. Eng. Manuf.*, Vol. 13, 2012, pp. 759–764.

24. Jones, D., Treloar, L., 'The Properties of Rubber in Pure Homogeneous Strain', *J. Phys. Appl. Phys.*, Vol. 8, No. 11, 1975, p. 1285.

25. Nicholson, D., Nelson, N., Lin, B., & Farinella, A., 'Finite Element Analysis of Hyperelastic Components', 1998.

26. Duncan, B., Maxwell, A., Crocker, L., & Hunt, R., 'Verification of Hyperelastic Test Methods.', 1999.

27. Sasso, M., Palmieri, G., Chiappini, G., & Amodio, D., 'Characterization of Hyperelastic Rubber-Like Materials by Biaxial and Uniaxial Stretching Tests Based on Optical Methods', *Polym. Test.*, Vol. 27, No. 8, 2008, pp. 995–1004.